

Article

Dynamics-Based Thermal Analysis of High-Speed Angular Contact Ball Bearings with Under-Race Lubrication

Jintao Lei, Bing Su *, Shuailong Zhang, Haisheng Yang and Yongcun Cui

School of Mechatronics Engineering, Henan University of Science and Technology, Luoyang 471003, China; m18800733295@163.com (J.L.); zsl18436097960@163.com (S.Z.); yhs1975@163.com (H.Y.); 9906172@haust.edu.cn (Y.C.)

* Correspondence: subing@haust.edu.cn; Tel.: +86-037964231479

Abstract: The paper mainly studied the temperature rise characteristics of under-race lubricated high-speed angular contact ball bearings under operational conditions from the perspective of dynamics. The steady-state calculation model of the bearing was established using a thermal network method in consideration of the influence factor of friction power consumption in bearing components based on a dynamic model. Following this, the steady-state change characteristics of the bearing were obtained by solving a thermal balance equation. Through this process, the influence laws of bearing rotation speed, oil supply, and environmental temperature on the friction temperature rise of the bearing were analyzed. Finally, the finite element analysis software ANSYS was employed to provide comparative verification. The results showed that the bearing temperature nonlinearly increased with the increase in inner ring rotation speed, and when it approached a certain critical value, the outer ring temperature exceeded the inner ring temperature. It had an obvious effect on controlling the temperature rise of the bearing inner ring by way of increasing the quantity and reducing the temperature of the lubricating oil supply. Comparative verification showed that the speed–temperature variation tendency from the dynamics-based thermal analysis well agrees with that of the finite element analysis.

Keywords: dynamics; friction power consumption; thermal network method; under-race lubrication



Citation: Lei, J.; Su, B.; Zhang, S.; Yang, H.; Cui, Y. Dynamics-Based Thermal Analysis of High-Speed Angular Contact Ball Bearings with Under-Race Lubrication. *Machines* **2023**, *11*, 691. <https://doi.org/10.3390/machines11070691>

Academic Editors: Thomas Hagemann and Hubert Schwarze

Received: 23 May 2023

Revised: 25 June 2023

Accepted: 27 June 2023

Published: 1 July 2023



Copyright: © 2023 by the authors. Licensee MDPI, Basel, Switzerland. This article is an open access article distributed under the terms and conditions of the Creative Commons Attribution (CC BY) license (<https://creativecommons.org/licenses/by/4.0/>).

1. Introduction

The big thrust-to-weight ratio and high power output of contemporary advanced aero engines are the current design and development trends. High-speed spindles present new issues and higher requirements for spindle bearing lubrication. The bearing produces a lot of heat when it operates regularly, including heat from friction caused by different friction pairs and heat from the viscous dissipation of lubricants. Some academics have proposed the use of under-race lubrication, which uses less oil and has positive effects on lowering the temperature in the bearing cavity, to optimize the heat dissipation of bearings at a high velocity of rotation. Therefore, it is important to research the under-race lubricated angular contact ball bearings' characteristics of temperature rise.

Gupta et al. [1] proposed a dynamic system based on ordinary differential equations to study the motion of bearing rolling elements. They studied the interaction between rolling element cages and raceway cages in theory and experiments and considered the cage imbalance and the dynamic pressure of the oil film between the guide ring and the cage. Han et al. [2] established a series of nonlinear dynamic models to study the slip behavior of angular contact bearings and roller bearings and the vibration characteristics of the rotor-bearing system. Through a combination of dynamic analysis and thermal elastohydrodynamic lubrication studies, Wang et al. [3] investigated the effects of rotational speed and external load on oil film thickness, temperature, and power loss. Palmgren et al. [4] carried out friction torque tests using different kinds and sizes of bearings and obtained the empirical formula of bearing friction torque by regression analysis and fitting

the collected test data. On the basis of Palmgren's method, Harris et al. [5] adjusted the general calculation method of bearing friction power consumption using an experiment and presented a local heat generation calculation method taking the six elements of rolling bearing friction into account. Wang et al. [6] obtained the temperature rise distribution of the bearing by calculating the heat generation and heat transfer of the bearing and carrying out finite element simulation. Sun et al. [7] analyzed the influence of speed on bearing temperature and studied the relationship between oil–air lubricated oil inlet speed and bearing heat generation. Yan et al. [8,9] focused on the friction loss and temperature rise of the bearing system. Bian et al. [10] studied the influence of bearing temperature on bearing axial stiffness. Using the finite element method, Tarawneh et al. [11] investigated the temperature distribution of the bearing components, friction heat generation, and surface temperature of the bearing box. Gentle et al. [12] considered the sliding state of high-speed ball bearings under the lubrication conditions of rich oil and poor oil. The test results show that a proper degree of poor oil can improve the overall sliding degree of bearings, which may be due to the reduction in lubricating oil drag resistance. Nicolas et al. [13] used the thermal network method in the temperature field analysis of sliding bearings. Jeng et al. [14] studied the effect of preload, oil quantity, air flow rate, and rotational speed on bearing temperature rise based on the oil–gas lubrication experiment of high-speed ball bearings. Flouros et al. [15] obtained the correlation between bearing heat generation and outer ring temperature after testing ball bearings and bearing chambers of a turbine engine and considering the influence of oil inlet direction and axial load direction. According to the heat transfer experiment of an aero engine bearing box and by simulating the oil condition in a typical high-temperature bearing of a turboshaft engine, Yuan [16] obtained the heat transfer law in the bearing box and the influence of the heat transfer coefficient on the bearing DN value ($DN > 3 \times 10^6$, bore diameter (mm) \times rotating speed (rpm)), lubricating oil flow, and oil supply temperature. Taking into account the effect of lubricating oil and thermal expansion, Zheng et al. [17,18] established a thermal grid analysis model of bearings and analyzed the factors that caused the temperature rise of bearings. Liu et al. [19] used the finite element software ANSYS simulation and verified the influence of load and speed on bearing temperature rise. Hu et al. [20] completed the temperature field analysis of angular contact ball bearings by finite element method and carried out experimental verification. It was concluded that the ball temperature among the bearing components was the highest, followed by the inner ring temperature, and the outer ring temperature was the lowest. Qin et al. [21] analyzed the main forms of heat transfer of rolling bearings and gave the heat generation calculation formulas of each element of rolling bearings. Chen et al. [22] analyzed the generation of each heat source of ball bearing and concluded that the rotational speed, axial load, and curvature radius coefficient of the inner ring groove had the main effect on the heat generation. Liang et al. [23] established the heat transfer model of hot nodes of rolling bearings and calculated the temperature of each node in consideration of the effect of bearing speed, load, centrifugal force, and spin on temperature rise. The results show that the heat generation of angular contact ball bearings is positively correlated with bearing rotation, load, centrifugal force, and spin. Ma et al. [24] established the friction torque model and the heat generation model of bearing, and then studied the influence of thread structure parameters and working condition parameters on friction heat generation. Zhang et al. [25] established the total needle bearing equation of a rocker arm on the basis of a dynamic analysis of rolling bearings and then studied the influence of working conditions on friction power consumption and the lubricant convection coefficient in consideration of the traction coefficient of the FVA-M reference lubricant.

In the above references, research on the temperature distribution of under-race lubrication bearing is rare, and there is a lack of research on the temperature distribution through dynamic analysis. In order to study the temperature characteristics of under-race lubrication bearing, this paper solves the dynamic equations and adopts the variable step integral algorithm (gear stiff) to carry out dynamic simulation analysis, thus obtaining the basic friction power consumption for thermal analysis, in which the influence of oil supply

temperature, oil supply amount, and bearing speed change on bearing temperature is also considered. It provides a theoretical basis for controlling the temperature of angular contact ball bearings under the ring.

2. Bearing Coordinate System

The research object is an angular contact ball bearing. In the dynamic analysis, it is assumed that the outer ring is connected with the ground, and the cage is guided by the inner ring. The center of mass of each part coincides with the center of shape, and the surface of each part is the ideal surface. The coordinate system can be established, which is shown in Figure 1.

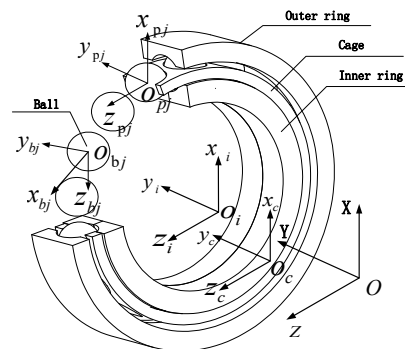


Figure 1. Bearing inertial coordinate system diagram.

(1) $\{O; X; Y; Z\}$ is a coordinate system fixed in space, in which the Y axis of the coordinate system coincides with the center line of the bearing, and the XZ plane of the static coordinate system is parallel to the radial plane passing through the center of the bearing.

(2) $\{O_{bj}; X_{bj}; Y_{bj}; Z_{bj}\}$ is the coordinate system of the center of mass of the rolling body, and J represents the j th rolling body. O_{bj} coincides with the center of the rolling body; Y_{bj} is finally parallel to the Y axis of the static coordinate system; Z_{bj} is along the radial direction of the bearing; X_{bj} is along the circumferential direction of the bearing, and the coordinate system moves along with the steel ball's center.

(3) $\{O_i; X_i; Y_i; Z_i\}$ is the coordinate system of the center of mass of the inner ring, O_i coincides with the geometric center of the outer ring, Y_i is along the rotation axis of the inner ring; and the XZ plane is parallel to the radial plane of the center of mass of the inner ring.

(4) $\{O_c; X_c; Y_c; Z_c\}$ is the centroid coordinate system of the outer ring, Y_c coincides with the rotation axis of the cage, the origin coincides with its centroid. The coordinate system moves along with the centroid of the cage.

(5) $\{O_{pj}; X_{pj}; Y_{pj}; Z_{pj}\}$ is the coordinate system of the j th pocket of the cage, which is fixed on the cage. Q_{pj} is located in the geometric center of the pocket of the cage. X_{pj} coincides with the radial direction of the bearing, and Z_{pj} is along the circumferential direction of the bearing.

2.1. Differential Equations for Bearing Dynamics

2.1.1. Differential Equations for the Dynamics of Steel Balls

Figure 2 shows the force of the j th steel ball. All calculation methods in the figure can be seen in [26]. The dynamic differential equation of steel balls based on Newton's law and classic Euler equations is as follows:

$$Q_{ej} \sin \alpha_{ej} - Q_{ij} \sin \alpha_{ij} + T_{\eta ej} \cos \alpha_{ej} - T_{\eta ij} \cos \alpha_{ij} - F_{R\eta ej} \cos \alpha_{ej} + F_{R\eta ij} \cos \alpha_{ij} + F_{H\eta ej} \cos \alpha_{ej} - F_{H\eta ij} \cos \alpha_{ij} + P_{S\zeta j} + P_{R\zeta j} = m_b \ddot{x}_b \quad (1)$$

$$Q_{ej} \cos \alpha_{ej} - Q_{ij} \cos \alpha_{ij} - T_{\eta ej} \sin \alpha_{ej} + T_{\eta ij} \sin \alpha_{ij} + F_{R\eta ej} \sin \alpha_{ej} - F_{R\eta ij} \sin \alpha_{ij} - F_{H\eta ej} \sin \alpha_{ej} + F_{H\eta ij} \sin \alpha_{ij} - F_{\eta j} - P_{S\eta j} - P_{R\eta j} = m_b \ddot{y}_b \quad (2)$$

$$T_{\xi ij} - T_{\zeta ej} - F_{R\xi ij} + F_{R\zeta ej} + F_{H\xi ij} - F_{H\zeta ej} + Q_{cj} - F_{Dj} - F_{\tau j} = m_b \ddot{z}_b \quad (3)$$

$$(T_{\xi ij} - F_{R\xi ij}) \frac{D_w}{2} \cos \alpha_{ij} + (T_{\zeta ej} - F_{R\zeta ej}) \frac{D_w}{2} \cos \alpha_{ej} - (P_{S\eta j} + P_{R\eta j}) \frac{D_w}{2} = I_b \dot{\omega}_{bx} + J_x \dot{\omega}_{xj} \quad (4)$$

$$(F_{R\xi ij} - T_{\xi ij}) \frac{D_w}{2} \sin \alpha_{ij} + (F_{R\zeta ej} - T_{\zeta ej}) \frac{D_w}{2} \sin \alpha_{ej} - G_{yj} - (P_{S\xi j} + P_{R\xi j}) \frac{D_w}{2} - J_y \dot{\omega}_{yj} = I_b \dot{\omega}_{by} - I_b \omega_{bjz} \dot{\theta}_{bj} \quad (5)$$

$$(T_{\eta ij} - F_{R\eta ij}) \frac{D_w}{2} + (T_{\eta ej} - F_{R\eta ej}) \frac{D_w}{2} - G_{zj} - J_z \dot{\omega}_{zj} = I_b \dot{\omega}_{bz} + I_b \omega_{by} \dot{\theta}_b \quad (6)$$

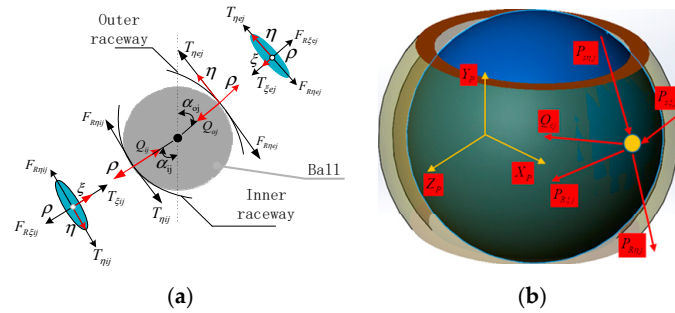


Figure 2. Schematic diagram of ball forces. (a) Force between steel ball and ring; (b) Force between steel ball and cage.

In the formula, the subscripts η and ζ , respectively, represent the short and long semi-axes of the ellipse where the steel ball contacts the raceway; m_b is the mass of the steel ball; $T_{\eta ej}$, $T_{\eta ij}$, $T_{\zeta ej}$, and $T_{\xi ij}$ are the drag force in the direction of the long and short axis at the contact between the steel ball and the inner and outer raceways; $F_{r\eta ej}$, $F_{r\eta ij}$, $F_{r\zeta ej}$, and $F_{r\xi ij}$ are the hydrodynamic friction forces in the contact entrance area between the steel ball and the raceway; $F_{h\eta ej}$, $F_{h\eta ij}$, $F_{h\zeta ej}$, and $F_{h\xi ij}$ are all horizontal components of hydrodynamic force acting on the center of the steel ball; $P_{S\eta j}$ and $P_{S\xi j}$ are the sliding friction forces on the surface of steel balls; $P_{r\eta j}$ and $P_{r\xi j}$ are the rolling friction forces on the steel ball surface; F_{d_j} is the aerodynamic resistance of the oil–gas mixture to a single steel ball; Q_{cj} is the collision force between the steel ball and the cage; $F_{\eta j}$ and $F_{\tau j}$ are the inertial force component during the movement of the steel ball; G_{yj} and G_{zj} are the components of the moment of inertia during the motion of the steel ball in the inertial coordinate system; J_x , J_y , and J_z are the components of the moment of inertia of the steel ball in the inertial coordinate system; I_b is the moment of inertia of the steel ball; ω_{bjx} , ω_{bjy} , and ω_{bjz} are the components of angular velocity of the steel ball in the inertial coordinate system, respectively; $\dot{\omega}_{bjx}$, $\dot{\omega}_{bjy}$, and $\dot{\omega}_{bjz}$ are the components of angular acceleration of the steel ball in the inertial coordinate system, respectively; \ddot{x}_{bj} , \ddot{y}_{bj} , and \ddot{z}_{bj} are the components of the acceleration of the steel ball centroid in the inertial coordinate system; and $\dot{\theta}$ is the rotation speed of the steel ball.

2.1.2. Dynamic Differential Equation of Cage

In the formulas, m_c is the mass of the cage; Q_{cxj} , Q_{cyj} , and Q_{czj} are the components of the collision force between the steel ball and the cage in the X , Y , and Z directions in the inertial coordinate system, respectively; φ_j is the position angle of the j th steel ball; d_m is the diameter of the bearing pitch; \ddot{x}_c , \ddot{y}_c , and \ddot{z}_c are the displacement accelerations of the cage in the inertial coordinate system; I_{cx} , I_{cy} , and I_{cz} are the moments of inertia of the cage in the inertial coordinate system; ω_{cx} , ω_{cy} , and ω_{cz} are the angular velocities of the cage in the inertial coordinate system; and $\dot{\omega}_{cx}$, $\dot{\omega}_{cy}$, and $\dot{\omega}_{cz}$ are the angular accelerations of the cage in the inertial coordinate system.

$$\sum_{j=1}^Z (P_{S\eta j} + P_{R\eta j} + Q_{cxj}) = m_c \ddot{x}_c \quad (7)$$

$$\sum_{j=1}^Z [(P_{S\xi j} + P_{R\xi j}) \cos \varphi_j + Q_{cyj}] = m_c \ddot{y}_c \quad (8)$$

$$\sum_{j=1}^Z [(P_{S\xi j} + P_{R\xi j}) \sin \varphi_j - Q_{czj}] = m_c \ddot{z}_c \quad (9)$$

$$\sum_{j=1}^Z \left[(P_{S\xi j} + P_{R\xi j}) \frac{D_w}{2} - Q_{cj} \frac{d_m}{2} \right] = I_{cx} \dot{\omega}_{cx} - (I_{cy} - I_{cz}) \omega_{cy} \omega_{cz} \quad (10)$$

$$\sum_{j=1}^Z (P_{S\eta j} + P_{R\eta j}) \frac{d_m}{2} \sin \varphi_j = I_{cy} \dot{\omega}_{cy} - (I_{cz} - I_{cx}) \omega_{cz} \omega_{cx} \quad (11)$$

$$\sum_{j=1}^Z (P_{S\eta j} + P_{R\eta j}) \frac{d_m}{2} \cos \varphi_j = I_{cz} \dot{\omega}_{cz} - (I_{cx} - I_{cy}) \omega_{cx} \omega_{cy} \quad (12)$$

2.1.3. Differential Equation of Inner Ring Dynamics

The bearing inner ring is mainly affected by the normal contact force, drag force, and hydrodynamic friction force of the contact inlet area of the steel ball to the inner ring.

$$F_x + \sum_{j=1}^Z (Q_{ij} \sin \alpha_{ij} - F_{R\eta ij} \cos \alpha_{ij}) = m_i \ddot{x}_i \quad (13)$$

$$F_y + \sum_{j=1}^Z [(Q_{ij} \cos \alpha_{ij} + F_{R\eta ij} \sin \alpha_{ij}) \cos \varphi_j + (T_{\xi ij} - F_{R\xi ij}) \sin \varphi_j] = m_i \ddot{y}_i \quad (14)$$

$$F_z - \sum_{j=1}^Z [(Q_{ij} \cos \alpha_{ij} + F_{R\eta ij} \sin \alpha_{ij}) \sin \varphi_j + (T_{\xi ij} - F_{R\xi ij}) \cos \varphi_j] = m_i \ddot{z}_i \quad (15)$$

$$M_y + \sum_{j=1}^Z \left[r_j (Q_{ij} \sin \alpha_{ij} - F_{R\eta ij} \cos \alpha_{ij}) \sin \varphi_j + \frac{D_w}{2} f_i T_{\xi ij} \sin \alpha_{ij} \cos \varphi_j \right] = I_{iy} \dot{\omega}_{iy} - (I_{iz} - I_{ix}) \omega_{iz} \omega_{ix} \quad (16)$$

$$M_z + \sum_{j=1}^Z \left[r_j (Q_{ij} \sin \alpha_{ij} - F_{R\eta ij} \cos \alpha_{ij}) \cos \varphi_j - \frac{D_w}{2} f_i T_{\xi ij} \sin \alpha_{ij} \sin \varphi_j \right] = I_{iz} \dot{\omega}_{iz} - (I_{ix} - I_{iy}) \omega_{ix} \omega_{iy} \quad (17)$$

where m_i is the mass of the inner ring; \ddot{x}_i , \ddot{y}_i , and \ddot{z}_i are the inner ring accelerations; I_{ix} , I_{iy} , and I_{iz} are the main moments of inertia of the inner ring ω_{ix} , ω_{iy} , and ω_{iz} are the angular velocities of the inner ring; $\dot{\omega}_{ix}$, $\dot{\omega}_{iy}$, and $\dot{\omega}_{iz}$ are the angular accelerations of inner ring; F_x , F_y , F_z , M_y , and M_z are the supporting forces and supporting moments acting on the inner ring, respectively; r_j is the radial distance from the contact point between the steel ball and the inner ring raceway to the center of mass of the inner ring; $r_j = 0.5d_m - 0.5D_w f_i \cos \alpha_{ij}$. f_i is inner ring raceway curvature radius coefficient. D_w is the diameter of the steel ball. $F_{R\eta ij}$ and $F_{R\xi ij}$ refer to the rolling friction force between the steel ball and the inner ring.

The drag force formula is $T_{\xi ij} = \mu Q_{ij}$, $T_{\xi ij}$ is the drag force between the steel ball and the rolling contact surface, and Q_{ij} is the contact force between the steel ball and the inner ring. The oil film drag coefficient μ is a variable, which can be obtained by experimentation. In this paper, FVA-M lubricating oil provided by Schaeffler Company in Germany is used, and the formula for calculating the drag coefficient of oil film is fitted from the experimental data according to the Gupta four-parameter model. The FVA-M lubricating oil drag coefficient measured on the tester in reference [27] can be expressed as the following formula:

$$\mu = (A + BS)e^{-CS} + D \quad (18)$$

$$\begin{cases} A = -0.5164\bar{W}^{-0.7102}\bar{U}^{-0.5353}\bar{T}^{-0.4159} \\ B = 4.6747 \times 10^4\bar{W}^{-0.0725}\bar{U}^{-0.2831}\bar{T}^{-0.079635} \\ C = 3.4129 \times 10^{-6}\bar{W}^{-0.021}\bar{U}^{-0.274}\bar{T}^{-0.4796} \\ D = 0.5164\bar{W}^{-0.7102}\bar{U}^{-0.5353}\bar{T}^{-0.4159} \end{cases} \quad (19)$$

where: \bar{W} is a dimensionless load parameter; \bar{U} is a dimensionless velocity parameter; \bar{T} is a dimensionless temperature parameter; and S is the slip–roll ratio at the contact between bearing elements.

3. Power Consumption Analysis Model of Bearing Assembly

Bearing Frictional Power Consumption

This paper uses the local method for calculation. For the local method, on the basis of Palmgren’s work, Harris et al. [5] modified the overall algorithm of bearing friction power consumption and proposed a local heat generation calculation method in consideration of the six factors of ball bearing friction power consumption. The friction power consumption of the angular contact ball bearing is comprised of ball-to-race interaction, ball-to-cage contact, cage-to-race contact, elastic hysteresis in the steel ball in a raceway, and churning loss and drag loss.

Friction Power Consumption Caused by Elastic Lag between Steel Ball and Raceway:

$$H_{Ei(e)} = \sum_{j=1}^Z M_{Ei(e)j}\omega_{bj} \quad (20)$$

$$M_{Ei(e)j} = \frac{D_m}{4}(1 - \gamma_0^2)\varphi_{i(e)j}\beta \quad (21)$$

$$\gamma_0 = D_w \cos \alpha_0 / d_m \quad (22)$$

where α_0 is the original contact angle; β is the elastic hysteresis coefficient and is equal to 0.007; ω_{bj} is the rotation angular velocity of the j th steel ball; and Z is the number of steel balls. $M_{i(j)}$ is the friction torque generated by the bearing, and $H_{i(j)}$ is the friction power consumption generated by the bearing.

$$\varphi_{i(e)j} = \frac{9}{128} \times \left(\frac{2k}{\pi\mu}\right)_{i(e)} \times \frac{1}{V_{i(e)}} \times \left(\frac{8}{3}\sum\rho_{i(e)}\right)^{2/3} \times E'^{1/3}F_{i(e)j}^{4/3} \quad (23)$$

$$\left(\frac{2k}{\pi\mu}\right)_{i(e)} = \frac{2K_{i(e)}(e)}{\pi} \left(\frac{\pi}{2k_{i(e)}^2L_{i(e)}(e)}\right)^{1/3} \quad (24)$$

$$V_{i(e)} = \left(\frac{2L_{i(e)}(e)}{\pi k_{i(e)}}\right)^{1/3} \quad (25)$$

$$k_{i(e)} = \frac{a_{i(e)}}{b_{i(e)}} \quad (26)$$

$$E' = \frac{4(1 - \mu_b)^2}{E_b} + \frac{4(1 - \mu_{i(e)})^2}{E_{i(e)}} \quad (27)$$

where F_{ij} and F_{ej} are the normal contact forces between the j th steel ball and the inner and outer ring raceways, respectively; $K_{i(e)}(e)$ and $L_{i(e)}(e)$ are elliptic integrals of the first and second kinds, respectively; μ_b is the Poisson’s ratio of steel balls; $\mu_{i(e)}$ is the Poisson’s ratio of the inner and outer rings of the bearing; $a_{i(e)}$ is the major semi-axis of the ellipse between the steel ball and the inner and outer rings; $b_{i(e)}$ is the short semi-axis of the ellipse

in contact between the steel ball and the inner and outer rings; E_b is the elastic modulus of the steel ball; $E_{i(e)}$ is the elastic modulus of the inner and outer rings of the bearing; and $\sum \rho_{i(e)}$ is the sum of the main curvature of the contact point between the steel ball and the inner and outer rings.

Friction Power Consumption Caused by Differential Sliding between Steel Ball and Raceway [28]:

$$H_{Di(e)} = \sum_{j=1}^Z M_{Di(e)j} \omega_{bj} \quad (28)$$

$$M_{Di(e)j} = \frac{D_m(1 - \gamma^2)}{2D_w} \Psi_{Di(e)j} f_s \quad (29)$$

$$\Psi_{Di(e)j} = 0.04025 \times \frac{U_{i(e)}}{r_{ci(e)}} \times \left(\frac{3E'}{8\sum \rho_{i(e)}} \right)^{2/3} \times F_{i(e)j} \quad (30)$$

$$U_{i(e)} = \left(\frac{2k_{i(e)}^2 L_{i(e)}}{\pi} \right)^{1/3} \quad (31)$$

$$r_{ci(e)} = \frac{f_{i(e)} D_w}{0.5 + f_{i(e)}} \quad (32)$$

$$r_{ci(e)} = \frac{f_{i(e)} D_w}{0.5 + f_{i(e)}} \quad (33)$$

where $f_{i(e)}$ is the radius coefficient of curvature of the groove of the inner and outer rings of the bearing and f_s is the sliding coefficient of friction.

Friction Power Consumption Caused by Steel Ball Spin Sliding:

$$H_{Si(e)} = \sum_{j=1}^Z M_{Si(e)j} \omega_{si(e)j} \quad (34)$$

$$M_{Si(e)j} = \frac{3}{8} \times f_s \times \sum \left(L_{i(e)}(e) a_{i(e)j} F_{i(e)j} \sin \alpha_{i(e)j} \right) \quad (35)$$

where $\alpha_{i(e)j}$ is the actual working contact angle between the j th steel ball and the inner and outer ring raceways and $\omega_{si(e)j}$ is the j th steel ball spin angular velocity.

Friction Power Consumption Caused by Contact between Cage and Guide Surface:

$$H_{cr} = 1.38 \times 10^{-7} W f_c n_{i(e)c} \varepsilon D_{2i(e)} (1 - r)^2 \times 10^{-3} \omega_c \quad (36)$$

where $n_{i(e)c}$ is the rotational speed of the ferrule relative to the cage; ω_c is the cage rotation angular velocity; ε offset of the cage center to the bearing center; $D_{2i(e)}$ is the diameter of the guide ferrule flange; W is the cage weight; $r = D_w \cos \alpha_0 / d_m$, where α_0 is the original contact angle.

Friction Power Consumption between Steel Ball and Cage:

$$H_{cb} = \frac{d_m}{4} (1 - r^2) \sin \left[\alpha_0 + \arctg \left(\frac{D_w \sin \alpha_0}{r_1} \right) \right] W f_c \omega_b \quad (37)$$

where $r_1 = \frac{d_m}{2} (1 - r)$; W is the weight of the cage; and f_c is the coefficient of sliding friction.

Friction Power Consumption Caused by Viscous Loss of Oil Film:

$$H_{oil} = 6.35 \alpha_{oil} S_n \frac{d_m}{2} \sum_{Z=1}^Z \left[\left(\frac{H_e + H_i}{2} \right) (a_e + a_i) \right] \omega_c \quad (38)$$

where $H_{i(e)}$ is the thickness of the oil film; α_{oil} is the viscosity coefficient; S_n is the sufficient lubrication coefficient. The oil film lubrication coefficient can be taken as $a_{i(e)}$ which is the contact ellipse major axis.

Total Friction Power Consumption:

The total energy power consumption of angular contact ball bearings caused by friction during operation is:

$$H = H_{Ei(o)} + H_{Di(o)} + H_{Si(o)} + H_{cr} + H_{cb} + H_{oil} \quad (39)$$

4. Thermal Network Method

During this study, through adopting the under-race lubrication method, the lubricating oil was transported to the inner race through the centrifugal force generated by the high-speed rotation of the shaft system. The friction power consumption caused by the bearing will eventually be dissipated by heat conduction and convection heat exchange when thermal radiation is being ignored. When the thermal network method is used to analyze the steady-state temperature field of the bearing system, the appropriate thermal nodes are selected first, then the heat transfer relationship of each component is determined. The thermal network relationship diagram is then established, and finally the thermal network linear equation system is established. The steady-state temperature values of each node are obtained by solving linear equations. Table 1 shows the basic structural parameters of bearings.

Table 1. Basic structural parameters of bearings.

Parameters	Symbol	Value
Outer ring diameter	D	62 mm
Inner ring diameter	d	30 mm
Bearing width	B	16 mm
Pitch diameter	dm	46 mm
Contact angle	α	30 °C
Steel ball diameter	Dw	9.525 mm
Number of steel balls	Z	11

4.1. Node Division of Thermal Network

As shown in Figure 3, 10 thermal nodes are selected in the angular contact ball bearing system, in which node T1 is the steel ball temperature; node T2 is the bearing inner ring raceway contact point temperature; node T3 is the bearing inner ring temperature; node T4 is the spindle temperature; node T5 is the bearing outer ring raceway contact point temperature; node T6 is the bearing housing temperature; and node T7 is the bearing housing temperature. In addition, node T8 and node Ta1, respectively, represent ambient temperature and lubricant temperature.

4.2. Thermal Resistance Calculation

According to the selection of nodes in Figure 3 and the heat transfer relationship between nodes, the thermal network analysis diagram can be obtained as shown in Figure 4.

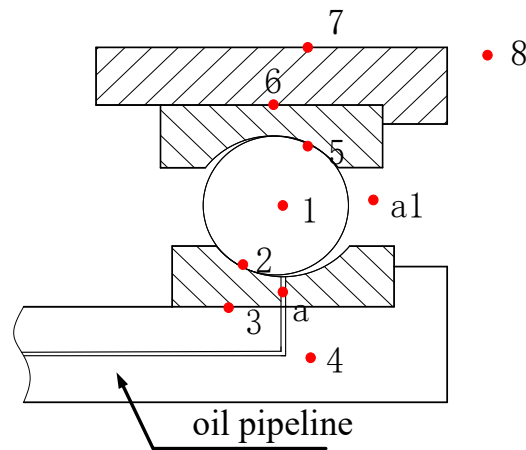


Figure 3. Thermal network node graph.

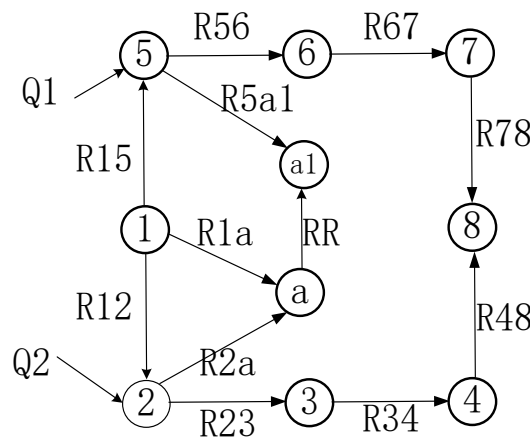


Figure 4. Thermal network analysis diagram.

4.2.1. Thermal Conductivity and Resistance

For the bearing inner ring, outer ring, and bearing block, it can be regarded as circular ring heat conduction, and the calculation formula is as follows [29]:

$$R = \frac{\ln(d_o/d_i)}{2\pi kl} \tag{40}$$

where d_o is the outer diameter of the ring, d_i is the inner diameter of the ring, k is the thermal conductivity of the material, and l is the characteristic length. Contact thermal resistance between the steel ball and raceway is [30]:

$$R = \frac{1}{\pi} \left(\frac{a}{b}\right) \frac{1}{ka\sqrt{pe}} \tag{41}$$

where a and b are steel balls and long and short semi-axes rolling to the contact area, respectively; k is the thermal conductivity; $pe = a\rho V_c C_p / k$ is Peclet number, where V_c is characteristic rotation speed and C_p is the specific heat capacity of lubrication.

4.2.2. Convective Thermal Resistance

Convective thermal resistance of a solid surface is usually expressed by the following formula:

$$R = \frac{1}{h_v S_d} \tag{42}$$

where h_v is the surface convective heat transfer coefficient and S_d is the convective heat transfer area. For the solution of h_v , please refer to [30].

For the lubricating oil to enter the bearing cavity to absorb energy, the calculation method is as follows [30]:

$$H = (T_{a1} - T_a)\rho_{oil}L_{oil}C_p \quad (43)$$

where T_{a1} is the oil outlet temperature, T_a is the oil inlet temperature, ρ_{oil} is the lubricating oil density, and L_{oil} is the lubricating oil flow rate.

The thermal grid method is based on the theory of heat transfer and takes the energy conservation theorem as the core. For establishing the heat balance equation, it is assumed that there is no heat exchange between 2 parts that are not in direct contact [19].

Based on the generalized ohm theorem, when calculating the steady-state heat transfer, the inflow heat of each node is equal to the outflow heat [30].

$$H_f + H_V + H_d = 0 \quad (44)$$

where H_f is the bearing heat production; H_V is the heat exchanged by thermal convection; and H_d is the heat exchanged by heat conduction.

The heat balance equation between nodes is [30]:

$$\sum \frac{T_X - T_y}{R_{xy}} = H_f \quad (45)$$

where T_X is the temperature between nodes and R_{xy} is the thermal resistance between nodes.

4.3. Establishment of Heat Balance Equations

The heat balance equations can be listed according to the thermal network analysis diagram, in which $Q1$ is the heat generation between the steel ball and the outer raceway and $Q2$ is the heat generated between the steel ball and the inner raceway. Since the heat generated at the contact point of the inner and outer raceways accounts for most of the heat generated by the bearing, the viewpoint put forward by Burton and Steph can make the heat generated at the contact point flow into the ring and the steel ball according to the ratio of 1:1 and at the same time simplify the heat source as the heat generated between the steel ball and the inner and outer raceways. $Q1$ and $Q2$ are calculated as follows:

$$\begin{aligned} Q1 &= \sum_{j=1}^Z H_{rej} + \sum_{j=1}^Z H_{dej} + \sum_{j=1}^Z H_{sej} + 0.5(H_{oil} + H_{cL} + H_c) \\ Q2 &= \sum_{j=1}^Z H_{rij} + \sum_{j=1}^Z H_{dij} + \sum_{j=1}^Z H_{sij} + 0.5(H_{oil} + H_{cL} + H_c) \end{aligned} \quad (46)$$

The linear equations for heat source, thermal resistance, and node temperature are established above, in which the ambient temperature node 8 and the oil supply node $Ta1$ are known. The Gauss–Seidel iterative method is used to solve the equations and obtain 8 unknown node temperatures.

5. Result

5.1. Calculation and Analysis of Bearing Power Consumption

5.1.1. Influence of Bearing Rotation Speed on Friction Power Consumption

Figures 5 and 6 show the change laws of various types of friction power consumption inside the bearing with the variation in bearing rotation speed. The working conditions of the bearing include an axial load of $Fa = 3000$ N and a radial load of $Fr = 780$ N. Figure 5 shows the effect of bearing rotation speed on friction power consumption.

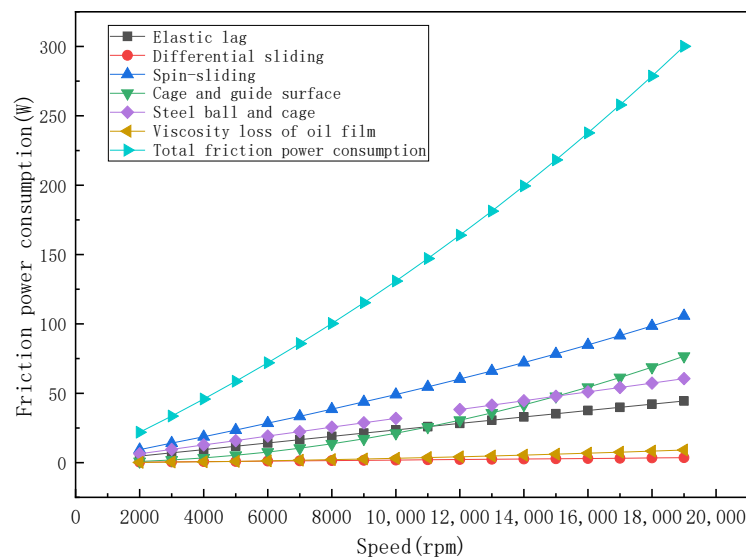


Figure 5. The effect of bearing rotation speed on various types of friction power consumption.

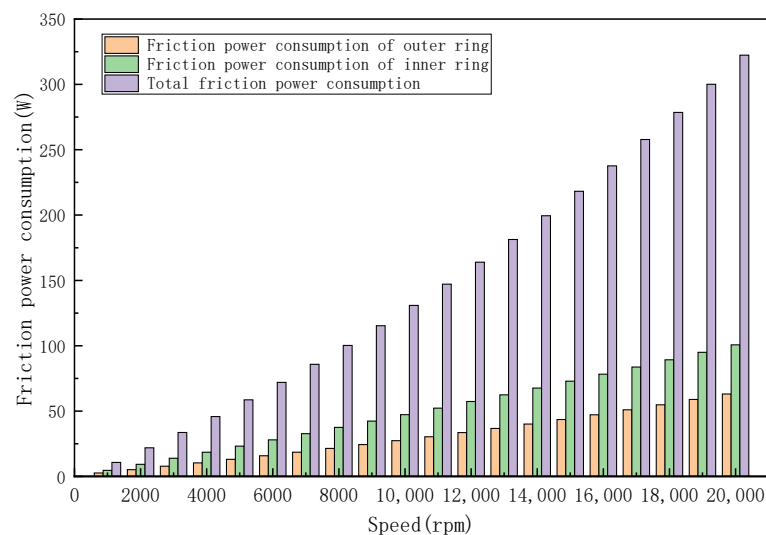


Figure 6. The effect of friction power loss by bearing rotation speed.

As the rotation speed increases, the various friction power consumptions of the bearing also increase. However, the increase resulting from the rolling element's spin sliding along the raceway is more noticeable than the increase in other friction power consumptions. The rolling element's spin-sliding friction is the main cause of the increase in friction power consumption, which is much greater than the friction caused by the elastic hysteresis rolling friction, differential sliding friction, friction between the rolling element and cage, and viscosity loss of oil film.

As shown in Figure 6, the friction power consumption between the inner ring and the balls is greater than that between the outer ring and the balls, and the total friction power consumption of the bearing shows an obvious upward trend with the increase in bearing rotation speed, which is mainly due to the friction of all parts of the bearing increasing with the increase in bearing rotation speed.

5.1.2. Effect of Axial Load on Friction Power Consumption

In order to analyze the influence of different axial loads on friction power consumption, the value of bearing rotation speed is set to 10,000 rpm while the radial load is fixed to the

constant 780 N, and the axial load is increased from 500 to 9000 N. The results are shown in Figures 7 and 8.

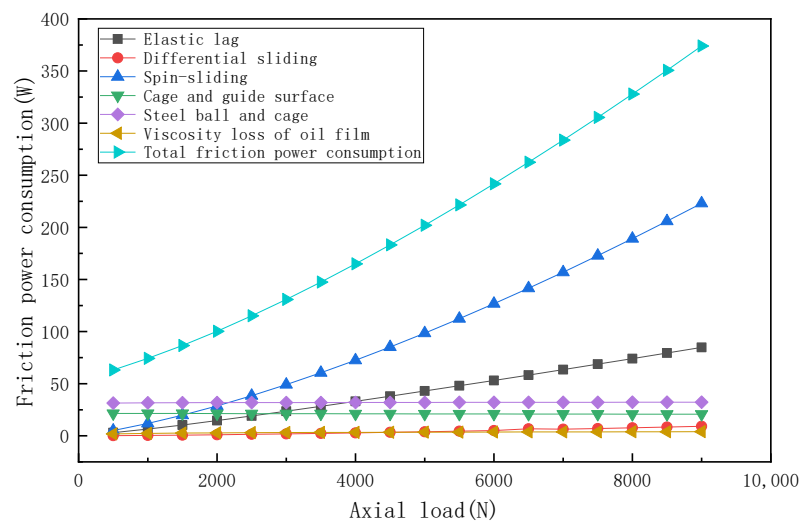


Figure 7. The effect of axial load on various types of friction power consumption.

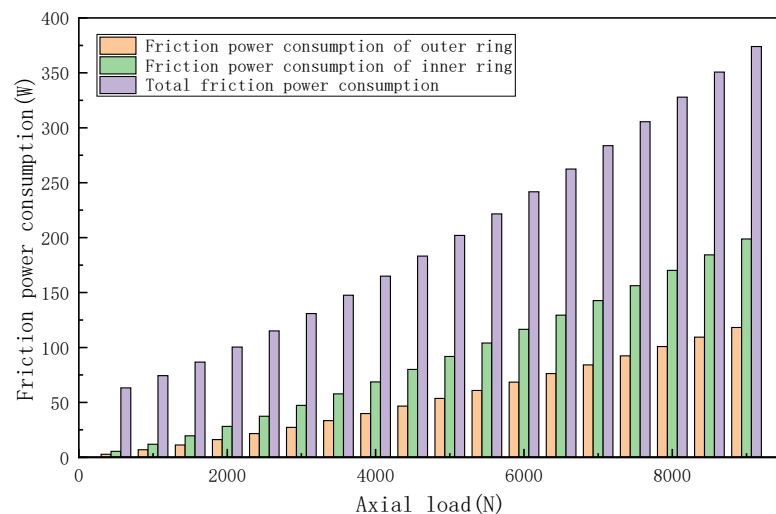


Figure 8. The effect of axial load on friction power consumption.

As can be seen from Figure 7, the greater the axial load, the more the friction power consumption of the bearing increases. Among them, the power consumption caused by the spin-sliding friction of the rolling elements is the largest, accounting for more than 50%, followed by the friction power consumption caused by elastic hysteresis, while the friction power consumption between the cage and the steel ball and between the cage and the guide surface are basically unchanged and account for a small proportion. The reason is that with the increase in axial load, the contact angle increases, which leads to the increase in the spin-sliding of the rolling elements, while the power consumption of other frictions increases slightly.

From Figure 8, it can be seen that on the whole, the friction power consumption between the inner ring and the balls is greater than that between the outer ring and the balls. With the increase in axial load, the total friction power consumption of the bearing is also increased.

5.1.3. Influence of Radial Load on Friction Power Consumption

In order to analyze the influence of different radial loads on friction power consumption, the value of bearing rotation speed is set to 10,000 rpm while the axial load is fixed to the constant 3000 N, and the radial load is increased from 100 to 3100 N. The results are shown in Figures 9 and 10.

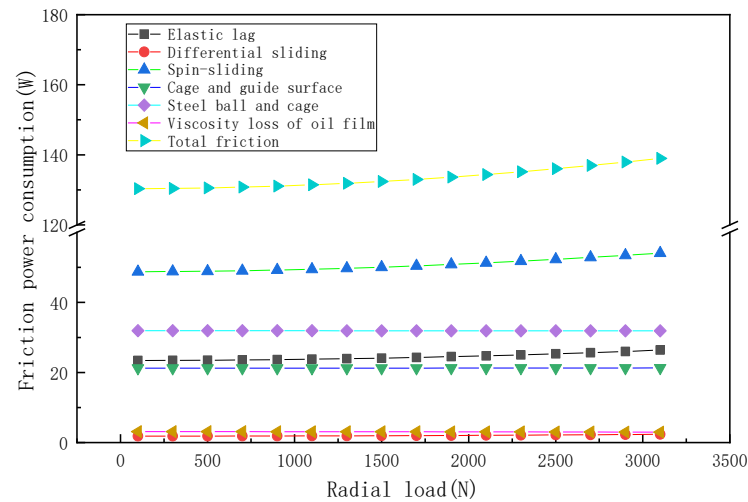


Figure 9. The effect of radial load on various types of friction power consumption.

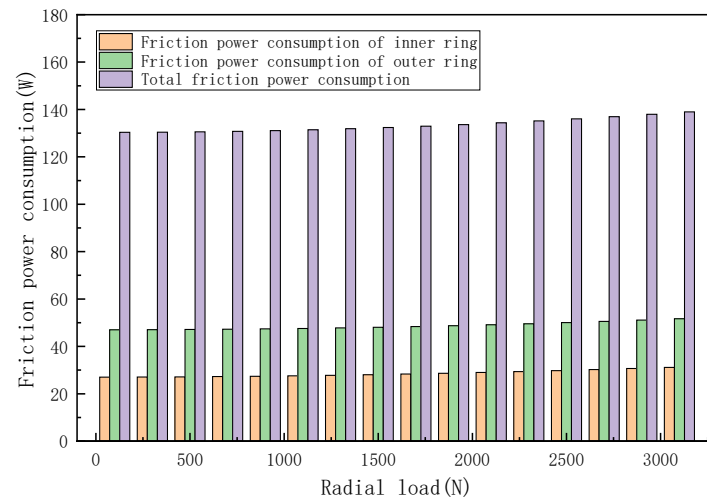


Figure 10. The effect of radial load on friction power consumption.

From Figure 9, when the radial load increases, the friction power consumption of each part in the bearing does not change obviously. Among them, the friction caused by spin-sliding only increased slightly and accounts for a large proportion, followed by the friction power consumption caused by steel balls and cages, followed by elastic hysteresis and friction power consumption caused by cage guide surfaces. Differential sliding and oil film agitation account for the smallest proportion. The friction power consumption of other parts remained in a relatively stable state.

As can be seen from Figure 10, as the radial load increases, the friction power consumption of the bearing inner and outer rings changes very little, from which it can be concluded that the radial load has little effect on the frictional power consumption of this bearing.

5.2. Temperature Simulation Analysis

For obtaining the relationship between the outer ring temperature and the rotation speed, the initial operating parameters are given as follows: the radial load 780 N, the axial

load 3000 N, and the ambient temperature 20 °C. The changing trend of the bearing outer ring temperature is observed.

As can be seen from Figure 11, before the bearing rotation speed reaches the certain critical value at approximately 11,000 rpm, the outer ring temperature does not increase obviously. When the bearing rotation speed increases, the bearing temperature increases more obviously. As this bearing has under-race lubrication, when the temperature of the inner and outer rings rises gradually beyond the oil temperature, the lubricating oil temperature will reduce the temperature of the inner ring. Therefore, when the bearing rotation speed reaches the critical rotation speed, the temperature of the inner and outer rings of the bearing rise sharply, and the temperature of the outer ring exceeds the inner ring temperature.

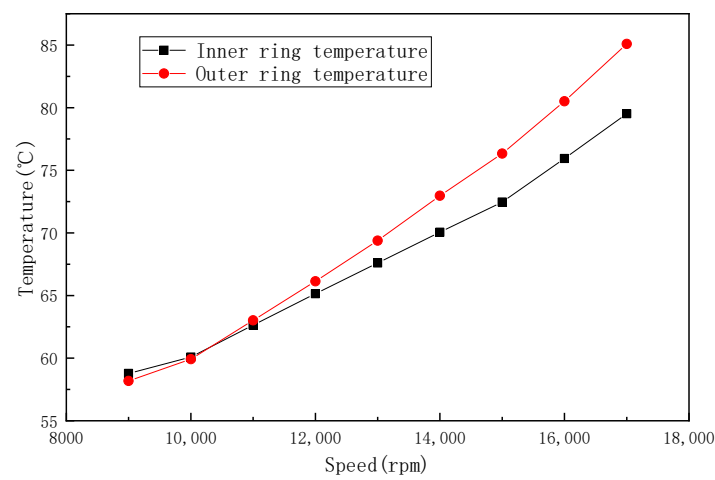


Figure 11. Change in node temperature with the rotating rotation speed ($F_a = 1000$ N).

The operational conditions of the bearing at various ambient temperatures are shown in Figure 12. As can be seen, each bearing node's steady-state temperature rises as the ambient temperature rises under the conditions of the radial load at 780 N and the axial load at 3000 N.

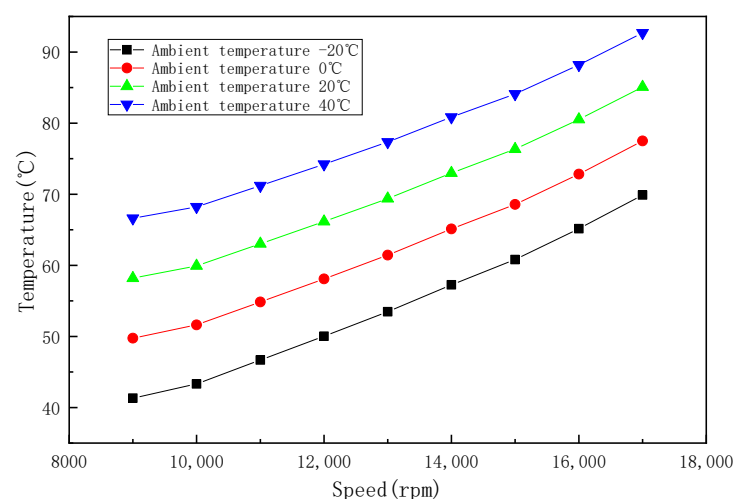


Figure 12. Effect of ambient temperature on bearing outer ring temperature.

Figure 13 illustrates the temperature variation trend of the outer ring of the bearing at different lubricating oil temperatures. The radial load of the bearing is fixed at 780 N and the axial load is 3000 N. The bearing rotational speed is from 9000 to 17,000 rpm. The figure shows that the temperature of the bearing outer ring increases with the increase in

bearing speed. On the other hand, when the rotational speed is a certain value, the higher the oil supply temperature, the higher the temperature the outer ring will be.

According to Figure 14, while the bearing is operating with a radial load of 780 N and an axial load of 3000 N, the rotation speed change is 9000–17,000 rpm, and the flow rate of oil is 1–10 L/min, allowing us to observe how the bearing's temperature changes. As can be seen from the figure, when the flow rate of oil is less than 2 L/min, the temperature of the bearing outer ring has an obvious upward trend. It is worth noting that when the oil flow rate allows, the temperature of the bearing outer ring shows a relatively linear change in the range of 2 L/min to 10 L/min of oil quantity. On the other hand, when the bearing rotation speed is fixed, the temperature of the bearing outer ring will not change obviously with the increase in the flow rate of oil.

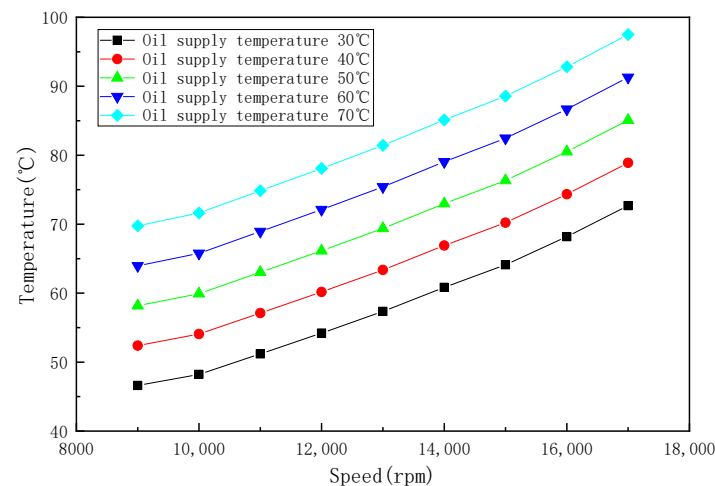


Figure 13. $F_a = 3000$ N and $n = 14,000$ rpm. Effect of oil supply temperature on bearing outer ring temperature.

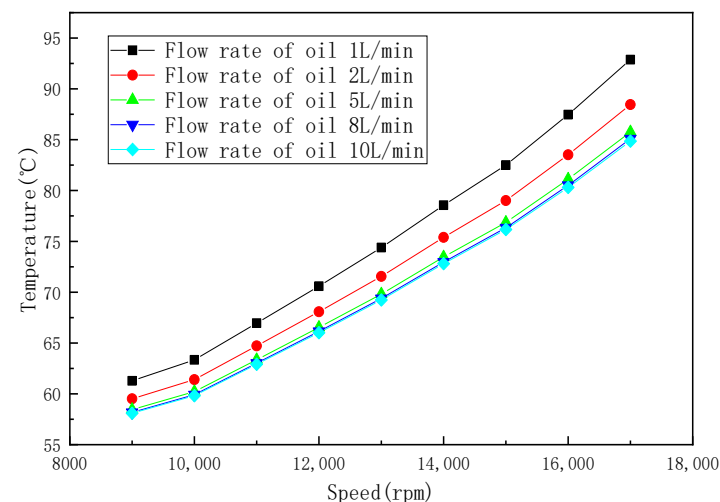


Figure 14. Effect of the flow rate of oil on bearing outer ring temperature.

6. Comparative Verification of the Dynamics-Based Thermal Analysis Results

6.1. Finite Element Comparative Analysis

Based on the finite element analysis theory, the thermal analysis model of the angular contact ball bearing was established using ANSYS software, and the power consumption calculation result was applied to the contact area to obtain the bearing temperature. The solution process is shown in Figure 15.

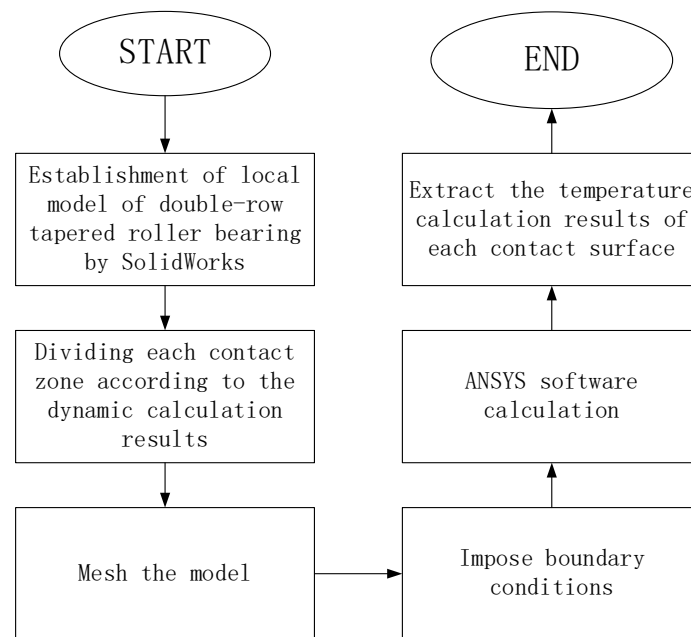


Figure 15. Finite element model solving process of angular contact ball bearing.

6.1.1. Establishment of Finite Element Model of Angular Contact Ball Bearing

The angular contact ball bearing's transition fillet and chamfer are omitted in modeling since they have little impact on the internal stress distribution and deformation. A cuboid is divided in the contact area between the ball and raceway of bearings, and its length and width are roughly equivalent to the long and short axes of the contact ellipse obtained by solving the Hertz contact problem in order to impose boundary conditions in the thermal analysis of bearings and avoid taking the whole raceway or the entire spherical surface as the target surface or contact surface. The model creates a total of 22 contact pairs when each ball develops contact pairs with the inner and outer rings, respectively. In order to reduce the calculation scale and ensure calculation accuracy, local mesh refinement is carried out in the contact area, as shown in the figure. The finite element model adopts eight-node solid 70 elements.

In order to facilitate the analysis, the following assumptions and simplifications were made for the model:

(1) The friction coefficient between contact surfaces, the linear expansion coefficient of materials, thermal conductivity, and other parameters are constant in the whole analysis process.

(2) As the thermal conductivity of the nylon cage is worse than that of bearing steel, its influence is ignored in the model.

(3) Burton and Staph [31] proposed that frictional heat is distributed 1:1 between the bearing ball and the ring, that is, half of the frictional heat enters the ball, and the other half enters the ring.

6.1.2. Influence of Rotation Speed on Bearing Temperature

Using a local heat generation model, friction heat generation model, and the convection coefficient obtained from Equation (42) as boundary conditions for temperature field calculation, bearing temperatures at different rotation speeds can be calculated. Figure 16 shows the distribution of bearing temperature. Table 2 shows the comparative analysis of the bearing inner ring temperature resulting from dynamics-based thermal analysis and from finite element simulation.

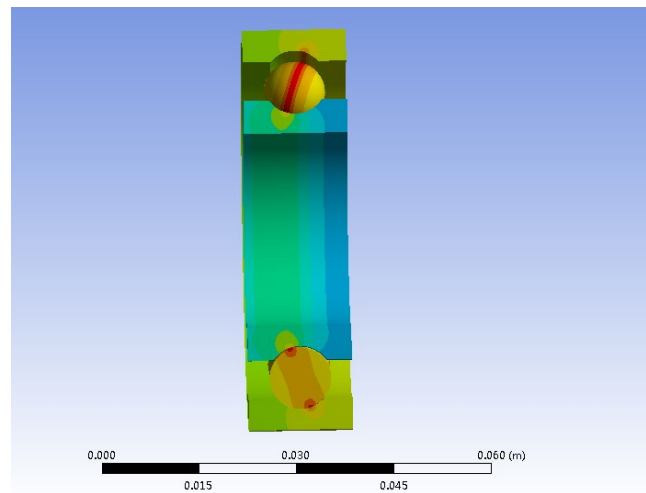


Figure 16. Finite element temperature distribution nephogram.

Table 2. The comparative results of outer ring temperature from dynamics-based thermal analysis (1) and finite element analysis (2).

Rotation Speed/rpm	Friction Power Consumption of Inner Ring/W	Friction Power Consumption of Outer Ring/W	Outer Ring Temperature (1)/°C	Outer Ring Temperature (2)/°C	Error (%)
9000	33.38	21.19	58.18	63.1	8.73
10,000	35.305	23.65	59.92	64.5	9.04
11,000	39.3	24.1	63.02	68.02	7.93
12,000	43.42	27.65	66.14	71	7.77
13,000	46.57	31.65	69.38	72	10.63
14,000	50.86	34.505	72.97	77.1	8.04
15,000	57.23	38.445	76.34	81.9	5.81
16,000	64.1	40.125	80.5	85	6.83
17,000	69.34	42.125	85.09	90	5.98

The comparative analysis of the bearing outer ring temperature under various operating conditions is illustrated in Figure 17. It can be seen that there is good agreement between the results from the finite element simulation and from dynamics-based thermal analysis, with a relative error of 10.63% at the highest and 5.81% at the lowest.

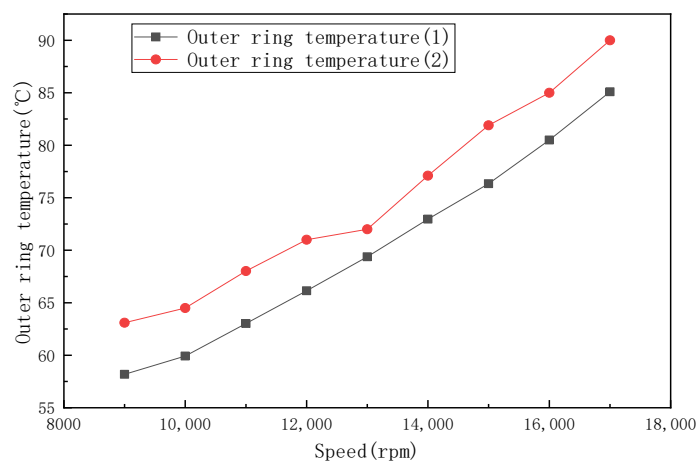


Figure 17. Simulation temperature comparison chart of outer ring.

The comparative verifications confirm the accuracy of the dynamics-based thermal analysis results presented in this paper.

7. Conclusions

The angular contact ball bearing was used as the research object in this paper, and under-race lubrication was chosen as the lubrication method. According to the bearing dynamics calculation, the bearing heat generation was calculated using the integral method. The steady-state temperature field was established using the thermal network method, and the temperature rise of each node under various operating conditions was forecasted and compared. Finite element analysis comparative verifications were carried out to evaluate the correctness of dynamics-based thermal analysis results.

1. The results showed the bearing temperature nonlinearly increased with the increase in inner ring rotation speed, and when it approached the certain critical value (approximately 11,000 rpm) the outer ring temperature exceeded the inner ring temperature. It had an obvious effect on controlling the temperature rise of the bearing inner ring by way of increasing the quantity and reducing the temperature of the lubricating oil supply.
2. The bearing temperature rise is analyzed by the bearing dynamics theory, and the friction power consumption between the bearing components is calculated more accurately. The friction power consumption of the bearing increases with the change in bearing rotation speed and axial load. On the other hand, the influence of radial load on friction power consumption is not obvious.
3. During the high-speed rotation of the angular contact ball bearing with the under-race lubrication, according to the temperature distribution of the outer ring, it is recommended that the flow rate of oil is 2–10 L/min because the temperature variation in the outer ring of the bearing is relatively average, which is more conducive to running with the bearing.
4. The temperature of the bearing node was obtained through a dynamic simulation. After comparative analysis, it was concluded that the difference between dynamic simulation analysis and finite element analysis results is less than 11%. The accuracy of this study was verified.

Author Contributions: Conceptualization, J.L. and B.S.; data curation, J.L. and S.Z.; formal analysis, J.L. and B.S.; funding acquisition, Y.C.; investigation, J.L., S.Z. and B.S.; methodology, B.S. and Y.C.; project administration, B.S. and H.Y.; resources, H.Y.; software, J.L.; supervision, Y.C. and B.S.; validation, Y.C. and S.Z.; writing—original draft, J.L. and B.S.; writing—review and editing, B.S., Y.C. and H.Y. All authors have read and agreed to the published version of the manuscript.

Funding: This research received was founded by the National Natural Science Foundation of China (52005158).

Data Availability Statement: The data used to support the findings of this study are available from the corresponding author upon request.

Conflicts of Interest: The authors declare no conflict of interest.

References

1. Gupta, P.K. Dynamics of rolling-element bearings-Part III: Ball bearing analysis. *J. Lubr. Technol.* **1979**, *101*, 312–318. [[CrossRef](#)]
2. Han, Q.K.; Chu, F.L. Nonlinear dynamic model for skidding behavior of angular contact ball bearings. *J. Sound Vib.* **2015**, *354*, 219–235. [[CrossRef](#)]
3. Wang, P.; Lei, C.L.; Zhou, B.C. Finite element analysis for thermal characteristics of high-speed angular contact ball bearing. *Appl. Mech. Mater.* **2013**, *397–400*, 126–130. [[CrossRef](#)]
4. Palmgren, A. *Ball and Roller Bearing Engineering*; Svenska Kullager Fabriken (SKF) Industries Incorporation: Philadelphia, PA, USA, 1959.
5. Harris, T.A.; Kotzalas, M.N. *Advanced Concepts of Bearing Technology: Rolling Bearing Analysis*; CRC Press, Taylor Francis Group: New York, NY, USA, 2006.

6. Wang, Y.L.; Wang, W.Z.; Li, Y.L.; Zhao, Z.Q. Lubrication and thermal failure mechanism analysis in high-speed angular contact ball bearing. *J. Tribol.* **2018**, *140*, 137–147.
7. Sun, Q.G.; Wang, Y.F.; Wang, Y. Numerical study on rolling bearing temperature field under the oil-air lubrication. *Appl. Mech. Mater.* **2014**, *487*, 580–584. [[CrossRef](#)]
8. Yan, C.; Zhao, M.; Lin, J. Fault signature enhancement and skidding evaluation of rolling bearing based on estimating the phase of the impulse envelope signal. *J. Sound Vib.* **2020**, *485*, 115529. [[CrossRef](#)]
9. Yan, C.; Lin, J.; Liang, K.X. Tacholeless skidding evaluation and fault feature enhancement base on a two-step speed estimation method for rolling bearings. *Mech. Syst. Signal Process.* **2022**, *162*, 108017. [[CrossRef](#)]
10. Bian, W.; Wang, Z.H.; Yuan, J.T. Thermo-mechanical analysis of angular contact ball bearing. *J. Mech. Sci. Technol.* **2016**, *30*, 297–306. [[CrossRef](#)]
11. Tarawneh, C.; Kypuros, J.; Navarro, L. Thermal modeling of a railroad tapered-roller bearing using finite element analysis. *J. Therm. Sci. Eng. Appl.* **2012**, *4*, 031002. [[CrossRef](#)]
12. Gentle, C.R.; Pasdari, M. Computer simulation of starvation in thrust-loaded ball-bearings. *Wear* **1983**, *92*, 125–134. [[CrossRef](#)]
13. Nicolas, J.A.M.; de Leon, F.G.; Alhama, F. Solution of Temperature Fields in Hydrodynamics Bearings by the Numerical Network Method. *Tribol. Int.* **2007**, *40*, 139–145. [[CrossRef](#)]
14. Jeng, Y.R.; Gao, C.C. Investigation of the ball-bearing temperature rise under an oil-air lubrication system. *Proc. Inst. Mech. Eng. Part J J. Eng. Tribol.* **2001**, *215*, 139–148. [[CrossRef](#)]
15. Flouros, M. Correlations for heat generation and outer ring temperature of high speed and highly loaded ball bearings in an aero-engine. *Aerosp. Sci. Technol.* **2006**, *10*, 611–617. [[CrossRef](#)]
16. Yuan, X.C.; Guo, H.; Wang, L.Y. Experiment study of heat transfer in aeroengine bearing chambers. *Appl. Mech. Mater.* **2011**, *86*, 448–453. [[CrossRef](#)]
17. Zheng, D.X.; Chen, W.F. Thermal performances on angular contact ball bearing of high-speed spindle considering structural constraints under oil-air lubrication. *Tribol. Int.* **2017**, *109*, 593–601. [[CrossRef](#)]
18. Zheng, D.X.; Chen, W.F.; Li, M.M. An optimized thermal net-work model to estimate thermal performances on a pair of angular con-tact ball bearings under oil-air lubrication. *Appl. Therm. Eng.* **2018**, *131*, 328–339.
19. Liu, X.W.; Wang, W.; Wang, Q.L. Study on Temperature Field of High-Speed Angular Contact Ball Bearings Based on ANSYS. *Modul. Mach. Tool Autom. Manuf. Tech.* **2015**, *3*, 13–15+20. (In Chinese)
20. Hu, X.Q.; Chen, W.F. Thermal Characteristics Analysis and Experiment for Angular Contact Ball Bearing. *J. Xi'an Jiao Tong Univ.* **2015**, *49*, 106–110. (In Chinese)
21. Qin, J.H.; Deng, C.Y.; Li, W. Heat Transfer Mechanism and Heat Calculation of Rolling Bearings. *Coal Mine Mach.* **2017**, *38*, 24–26. (In Chinese) [[CrossRef](#)]
22. Chen, G.C.; Wang, L.Q.; Gu, L. Heating analysis of the high-speed ball bearing. *J. Aerosp. Power* **2007**, *1*, 163–168. (In Chinese)
23. Liang, Q.; Liu, X.L.; Du, X. Analysis of Temperature Field in Angular Contact Ball Bearings. *Lubr. Eng.* **2015**, *40*, 37–41+45. (In Chinese)
24. Ma, S.J.; Liu, G.; Rui, T.T. A frictional heat model of planetary roller screw mechanism considering load distribution. *Mech. Based Des. Struct. Mach.* **2015**, *43*, 164–182. (In Chinese) [[CrossRef](#)]
25. Zhang, G.T.; Su, B.; Liu, F.B. Thermal Analysis Based on Dynamic Performance of Rocker Arm Full-Type Needle Bearings. *Lubricants* **2022**, *10*, 104. [[CrossRef](#)]
26. Sugimura, J.; Okumura, T.; Yamamoto, Y.; Spikes, H. Simple equation for elastohydrodynamic film thickness under acceleration. *Tribol. Int.* **1999**, *32*, 117–123. [[CrossRef](#)]
27. Ma, Y.; Su, B.; Liu, Y.Y. An Improvement on Traction Measurement System. In Proceedings of the 2018 International Conference on Computer, Communications and Mechatronics Engineering, Shanghai, China, 22–23 December 2018; Destech Publications: Lancaster, PA, USA, 2018; pp. 678–681.
28. Deng, S.E.; Li, X.L.; Wang, J.G. Friction al Torque Characteristic of Angular Contact Ball Bearings. *J. Mech. Eng.* **2011**, *47*, 114–120. (In Chinese) [[CrossRef](#)]
29. Yuan, A.S.; Wang, W.Z.; Wang, Y.L.; Zhao, Z.Q. Temperature rise of double-row tapered roller bearings analyzed with the thermal network method. *Tribol. Int.* **2015**, *87*, 11–22.
30. Neurouth, A.; Changenet, C.; Ville, F.; Arnaudon, A. Thermal modeling of a grease lubricated thrust ball bearing. *Proc. Inst. Mech. Eng. Part J J. Eng. Tribol.* **2014**, *228*, 1266–1275. [[CrossRef](#)]
31. Burton, R.A.; Staph, H.E. Thermally activated seizure of angular contact bearings. *ASLE Trans.* **1967**, *10*, 408–417. [[CrossRef](#)]

Disclaimer/Publisher’s Note: The statements, opinions and data contained in all publications are solely those of the individual author(s) and contributor(s) and not of MDPI and/or the editor(s). MDPI and/or the editor(s) disclaim responsibility for any injury to people or property resulting from any ideas, methods, instructions or products referred to in the content.